International Journal of Modern Manufacturing Technologies
ISSN 2067–3604, Vol. XIV, No. 3 / 2022
https://doi.org/ 10.54684/ijmmt.2022.14.3.205

WIND LOAD EVALUATION OF ROOF PHOTOVOLTAIC PANELS LOADED IN THE BOUNDARY LAYER WIND TUNNEL

Razvan Andrei Polcovnicu, Nicolae Taranu, Dragos Ungureanu, Sebastian Valeriu Hudisteanu

"Gheorghe Asachi Technical University of Iasi, Faculty of Civil Engineering and Building Services, Blvd. Dimitrie Mangeron 1, 700050, Iasi, Romania

Corresponding author: Razvan Andrei Polcovnicu, razvan-andrei.polcovnicu@student.tuiasi.ro

Abstract: Nowadays, more and more solar panel devices are mounted on the roofs. In some particular situations, the assessment of a structure in a higher energetic efficiency category (passive/active houses) may lead to the case of covering the entire roof with a system of photovoltaic panels. In these circumstances, an experimental study for testing the structural behaviour of the roof is mandatory to accurately estimate the true wind load. In this paper is presented an experimental setup based on two configurations of roofs, both made with photovoltaic panel systems, which are tested to wind actions. To maximize precision, the roof scaled models were designed in 3D modelling software and printed using a 3D printer. After the models were printed, they were instrumented with strain-gauge pressure sensors and prepared for the wind load tests.
Key words: solar radiation, PV panel, 3D printer, wind tunnel, roof system.

1. INTRODUCTION

Given the rapid development of solar energy technology, nowadays, there are increasingly more urban engineering projects based on solar energy for producing electric energy, domestic hot water supply and heating than ever before [1, 2]. However, due to the high building density in cities, in the near future, occlusion may reduce the solar equipment annual efficiency to a financially unfeasible degree. This issue can be addressed by installing various solar-powered devices on building roofs, or even by covering the entire surface of the roofs with this equipment [3]. Since solar concentrating systems usually have large windward surfaces and low structural rigidity, focus on wind load effect on structural design is needed to accurately estimate the true wind load on integrated roof solar devices [4, 5].

This paper focus on the experimental equipment required for testing several roof configurations loaded in various wind scenarios. Also, it is discussed the roof model selection method, the roof's characteristics, the 3D printer setup for manufacturing the scaled testing model and the simulation of wind field inside the boundary layer wind tunnel.

2. TEST EQUIPMENT

An experimental program has been developed in atmospheric boundary layer wind tunnel (SECO 2) in the Laboratory of Aerodynamics from the Faculty of Civil Engineering and Building Services in Iaşi, with the goal to evaluate the wind loading on two roof configurations. The SECO 2 wind research facility (Figure 1) consists in an open circuit boundary layer wind tunnel, having a transversal section of 1.4 m × 1.4 m and a total length of 8.8 m. The wind mean speed in the top part of the SECO 2 tunnel was limited at a maximum of 7.5 m/s, and the turbulence intensity at reference height was set in between the range 22% - 24%.

In the SECO 2 boundary layer wind tunnel the velocity profiles and the turbulence structures can be generated through various combinations of obstructions and ground roughness. The latter are used to accurately simulate the turbulent boundary layer flow of the natural wind, specific to the characteristics of the region where the construction is/will be located.

The SECO 2 boundary layer wind tunnel can therefore be used to determine the real flow in the vicinity of the building (e.g., to evaluate the wind loads) and to measure the velocity fields for complex topographic conditions (e.g., the flow around steep slopes).

Reliable simulations in the SECO 2 boundary layer wind tunnel impose a correct growth of the boundary layer and a scale models made of quality materials. Mean velocity profiles, power spectra, turbulence profiles and finally integral scales of turbulence can provide essential information for the design stage only if the data recorded from the tunnel is reliable.

The data acquisition system (DAQ), specifically designed for the SECO 2 boundary layer wind tunnel, consists in several items that allow the conversion of the physical forces into digital values that can be managed by a computer.

Fig. 1. The SECO 2 wind research facility

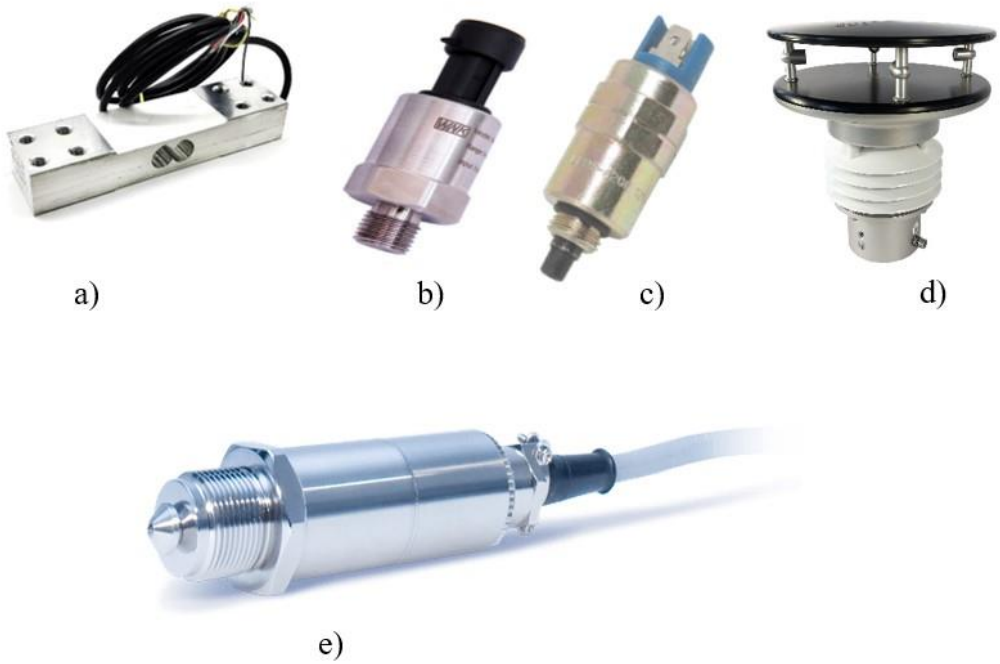

Fig.2. Sensors for boundary layer wind tunnels: a) Weight balanced sensors [12]; b) Pneumatic and hydraulic sensors [13]; c) Electromagnetic sensors [14]; d) Spring sensors [15]; e) Strain-gauge pressure sensors [16]

According to previous wind studies, the components comprise the DAQ and the selection of their properties has an important impact on the overall system behavior [6, 7].

The main components of the SECO 2 boundary layer wind tunnel DAQ can be divided in two main categories, as following:

➢Mechanics:

Designed to ensure that no friction forces are occurring and the monitored data are as close as possible to the ones specific to the building location.

➢Sensors or transducers:

The sensors are devices that convert the physical load in an electrical signal. The capability of the sensors to measure the force depends on the properties of the load and the sensor itself. The boundary layer wind tunnels can be equipped with various sensors [8]:

- Weight balanced sensors (Figure 2a)
- Pneumatic and hydraulic sensors (Figure 2b)
- Electromagnetic sensors (Figure 2c)
- Spring sensors (Figure 2d)
- Strain-gauge pressure sensors (Figure 2e)

➢The strain-gauge pressure sensors, also referred as load cells, are the most common ones, being able to generate the electrical signal trough the mechanical deformation that causes the applied force. The classical configuration consists in 4 strain gauges, disposed in a Wheatstone bridge arrangement that

converts the deformation into electrical signals. This configuration was chosen for the experimental set-up, since previous test proved that is both sensitive and accurate for classic and modern roof configurations [9, 10, 11].

➢ Electronic amplifiers:

The strain-gauge output signal is a weak signal of around a few millivolts thus, its power was increased by means of an amplifier in order to have a distinguishable signal in the analog to digital converter.

➢ Wires:

The electrical signal is transferred from the sensor to the amplifier and from the amplifier to the sensor by means of wires. The wires connected to the SECO 2 boundary layer wind tunnel DAQ are high quality and efficient.

3. ROOF MODEL

The 3D printer used to create the scaled testing model is Prusa i3 MK3 (Figure 3) [17]. The base and the Y axis of the printer are made with aluminum extrusion thus, eliminating the last of the structural threaded rods from the Mendel design and allowing for more complicated model designs [18]. During the printing stages, the ambient temperature sensor confirms a suitable environment temperature and detected no overheated electrical connections on the main board.

The first step of any 3D printing process is the 3D modelling. To maximize precision, the roof scaled models were designed in a 3D modelling software [19, 20]. Once the models were created, the slicing technique follows. Since the 3D printer cannot conceptualize the concept of three dimensions, the model was divided in layers in order for the printer to create the final product. Using the Prusa slicing software each layer of the roof models was scanned and the printer moving paths were determined. Also, the roof models "fill" degrees were imposed [21]. This "fill" asses the roof models with internal lattices and columns that help shape and strengthen the object. Once the models were sliced, it was sent off to the 3D printer for the actual printing process.

The printer acts generally the same as a traditional inkjet printer in the direct 3D printing process, where a nozzle moves back and forth while dispensing a wax or plastic-like polymer layer-by-layer, waiting for that layer to dry, and then adding the next level. It essentially adds hundreds or thousands of 2D prints on top of one another to make a three-dimensional object [22].

The first roof configuration chosen was printed directly as shown in Figure 4. On the other hand, some testing 3D models are impossible to create in one piece, due to their complexity.

Therefore, the second roof model was partitioned into several simpler parts (Figure 5).

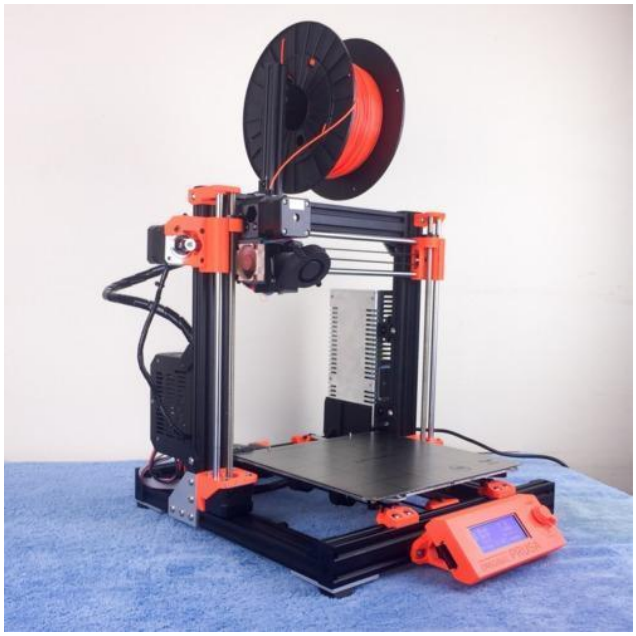

Fig. 3. 3D printer Prusa i3 MK3 [17]

After the parts were printed, the second roof model was fixed together.

For the testing models manufactured with the 3D printer, the scale was 1:20. The printing material was polylactic acid, also referred as polylactic acid or polylactide (PLA). The latter is a thermoplastic polymer made entirely from renewable resources (corn starch, potato starch, sugarcane and tapioca). The PLA used for the manufacturing of the roof models was provided by the manufacturer in filament form, with a diameter of 1.75 mm and possibility to connect directly to the printer extruder [23].

The fill density was set at the value of 15% and the fill pattern used was Gyroid (Figure 6) [24]. The length of the infill anchor was set to 2.5 mm and the maximum length allowed for it was 12 mm. More than that, the top and bottom fill pattern used was monotonic and the layer height was locked-in at the value of 0.15 mm. The only difference was the first layer height, which was set at 0.2 mm (the first layer is the most important because it represent the mounting of the executed model on the 3D printer printing base) [25].

4. SIMULATION OF WIND FIELD AND WORK CONDITIONS

Considering the geomorphic characteristics of the building location site in Iași, the class C landform wind field atmospheric boundary layer was simulated in the wind tunnel with grids, wedges, baffles and rough elements [27, 28, 29].

The wind speed profile is expressed by Equation 1:

$$V(z_g) = V_b\left(\frac{Z_g}{Z_b}\right)^{\partial} \quad (1)$$

where,

Z_b — standard reference height [m];

V_b — mean wind speed at standard reference height [m/s];
Z_g — height above the ground [m];
$V(z_g)$ — wind speed at height Z_g [m/s];
∂ — ground roughness index, in this study class C landform is simulated, and the value of ∂ is 0.22 according to the building load code.

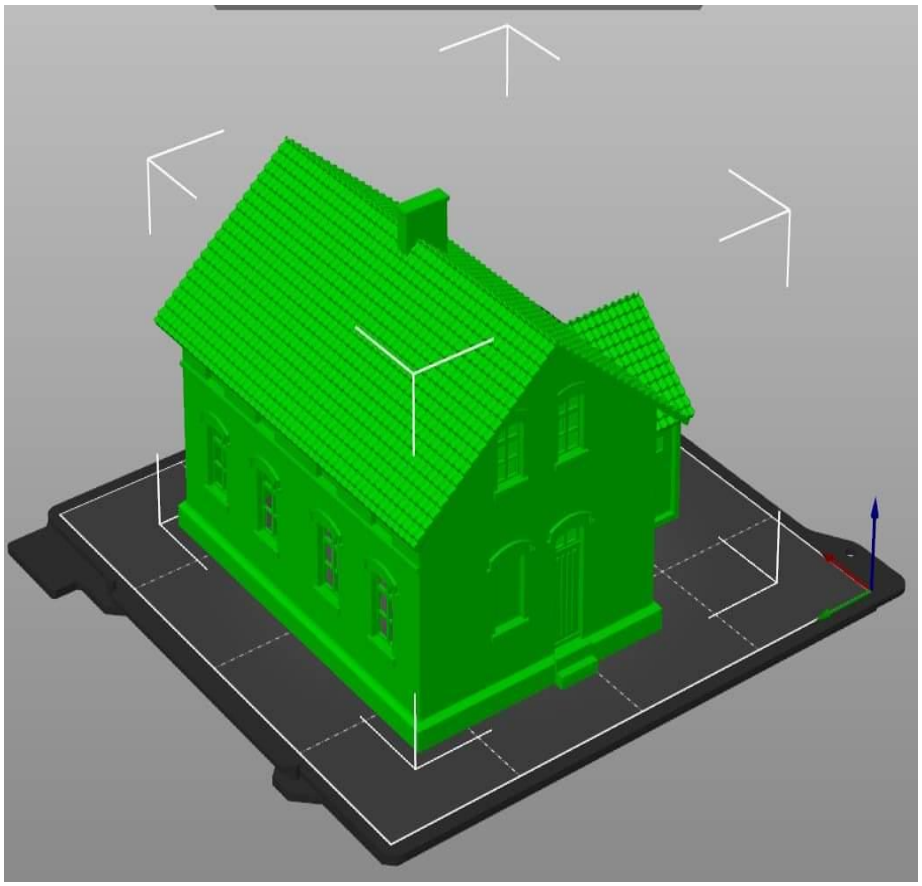

Fig. 4. First scaled roof testing model

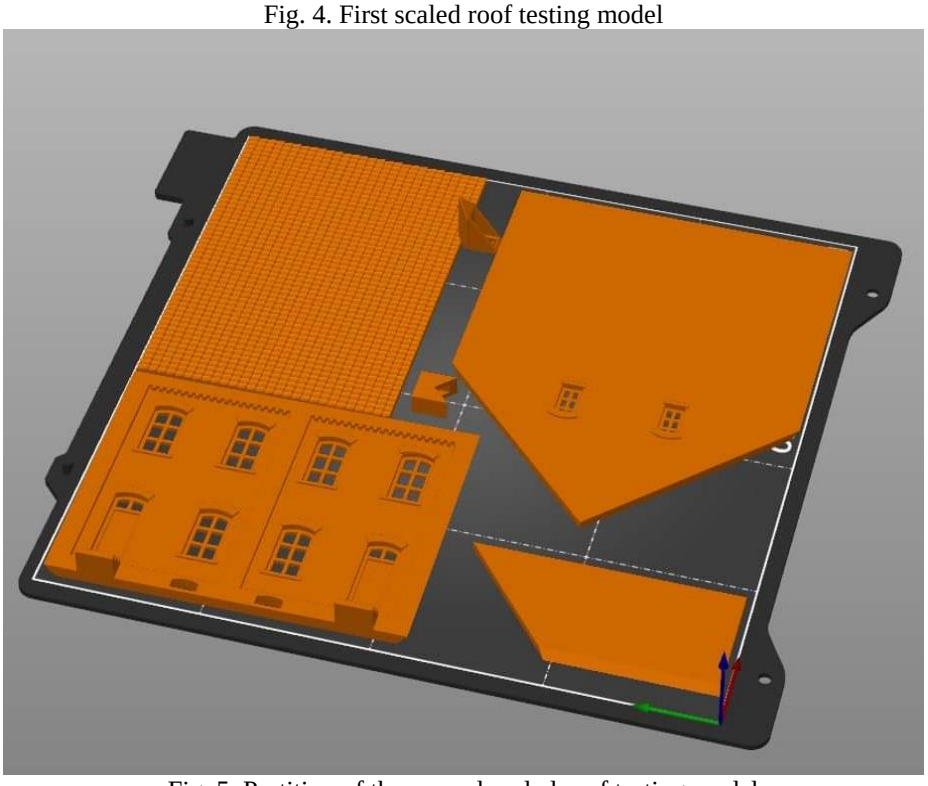

Fig. 5. Partition of the second scaled roof testing model

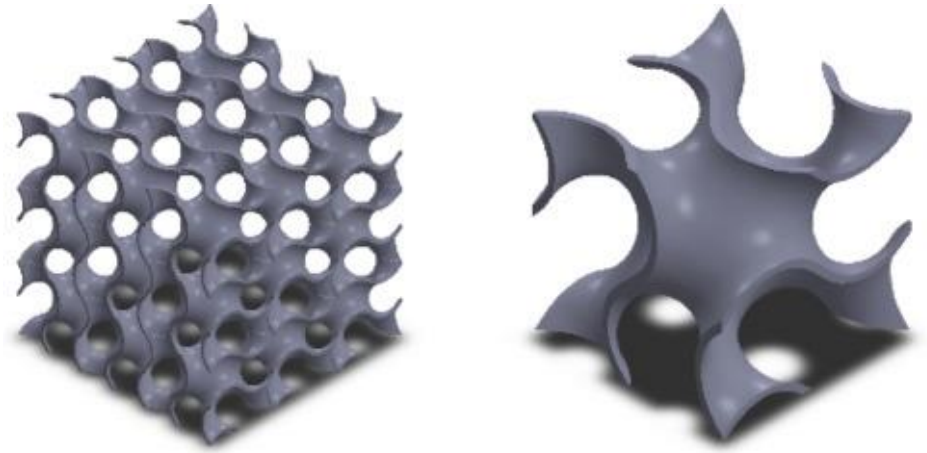

Fig. 6. Printed polymeric Gyroid cellular structure [26]

The distribution of wind field turbulence intensity, with height, is calculated using Equation 2:

$$I(z_g) = I_{10}\bar{I}(z_g) \quad (2)$$

where,
$I(z_g)$ — turbulence intensity at height Zg;
I_{10} — nominal turbulence intensity at 10 m, which is 0.23 corresponding to the roughness of class C landform;
∂ — the same as in Equation 1;
$\bar{I}(z_g)$ — is the height above ground, Z_g divided by 10 and to the power of minus ground roughness index, - ∂.

5. CONCLUSIONS

By performing the wind action study based on the envisaged experimental set-up, viable conclusions can be drawn regarding the behaviour of the roofs made with photovoltaic systems loaded in various wind scenarios. Upon these conclusions, the key ones may refer to the effect of roof and solar panel pitches, the optimum height-depth ratio and the recommended width-depth ratio on the pressure coefficients for different regions on the roof. Also, if necessary, fitting formulas for pressure coefficients on each roof region and pressure coefficient values for the design of roof photovoltaic system may be proposed. Thus, the design of the photovoltaic system roof shape and its geometrical characteristics can be optimised in order to avoid the apparition of roof zones susceptible to the wind loads.

6. ACKNOWLEDGEMENT

This work was supported by a grant of the Romanian Ministry of Education and Research, CCCDI-UEFISCDI, project number PN-III-P2-2.1-PED-2019-1294, within PNCDI III.

7. REFERENCES

1. Bergh, H., Tijdeman, H., (1965). *Theoretical and Experimental Results for the Dynamic Response of Pressure Measurement Systems*, National Aero- and Astronautical Res. Inst., Netherlands, Report NLR-TR F.238.
2. Cook, N.J., (1985). *The Designer's Guide to Wind Loading of Building Structures. Part 1: Background, Damage Survey, Wind Data and Structural Classification*, Build. Res. Establ. Report.
3. Holmes, J.D., (1984). *Effect of Frequency Response on Peak Pressure Measurements*, J. of Wind Engng. A. Ind. Aerodynam., 17, 1-9.
4. Holmes, J.D., Lewis, R.E., (1987). *Optimization of Dynamic-Pressure-Measurement Systems. I. Single Point Measurement*, J. of Wind Engng. a. Ind. Aerodyn., 25, 249-273.
5. Holmes, J.D., Lewis, R.E., (1987). *Optimization of Dynamic-Pressure-Measurement Systems. II. Parallel Tube Manifold Systems*, J. of Wind Engng. a. Ind. Aerodyn., 25, 275- 290.
6. Radu, A., Axinte, E., Teohari, C., (1986). *Steady Wind Pressures on Solar Collectors on Roofed Buildings*, J. of Wind Engng. a. Ind. Aerodyn., 23, 249-258.
7. Radu, A., Axinte, E., (1989). *Wind Forces on Structures Supporting Solar Collectors*, J. of Wind Engng. a. Ind. Aerodyn., 32, 93-100.
8. Ruscheweyh, H., Windhövel, R., (2011). *Wind Loads at Solar and Photovoltaic Modules for Large Plants*, 13th Internat. Conf. on Wind Engng. (ICWE13), Amsterdam, The Netherlands, https://www.ruscheweyh.de/assets/userfiles/publikationen/Wind-loads-at-Photovoltaic-modules.pdf, accessed: 17.01.2022.
9. Surry, D., Stathopoulos, T., (1977). *An Experimental Approach Economical Measurements of Spatially Averaged Wind Loads*, J. of Wind Engng. a. Ind. Aerodyn., 2, 385- 397.

10. Price, H., Lupfert, E., Kearney, D., et al., (2002). *Advances in parabolic trough solar power technology*, J. Sol. Energy Eng., 124 (2), 109–125.
11. Axinte, E., Taranu, N., Pescaru, R.A., (1996). *Studiu in tunel aerodinamic privind influenta anturajului constructiilor cu acoperis in panta asupra campului de presiuni induse de vant*, Conferinta nationala AICPS, Iasi, II, 7-12.
12. Manyi 1pc New 200kg Electronic Balance Platform Scale Load Cell Weight Weighing Sensor, Available from: https://www.joom.com/ro/products/5cbeb1318b2c3701013099d9, Accessed on: 04/02/2022.
13. Pneumatic and Hydraulic Pressure Sensor, Available from: https://m.made-in-china.com/product/Pneumatic-and-Hydraulic-Pressure-Sensor-with-4-20mA-0-5-4-5V-0-5V-Output-834615765.html, Accessed on: 04/02/2022.
14. Electromagnetic sensors, Available from: https://www.amazon.com/Sparex-Solenoid-189646m1-Ferguson-31403660364S/dp/B01N57O7, Accessed on: 04/02/2022.
15. HIM- digital and analog Measurement Devices, Available from: https://www.meteorologyshop.eu/en/sensors/climate-sensors/816/u-sonic-w6-spring-sensor-for-air-temperature-humidity-wind-air-pressure, Accessed on: 04/02/2022.
16. Tie Bar Strain Gauge, Available from: https://www.indiamart.com/proddetail/tie-bar-strain-gauge-20606884355.html, Accessed on: 04/02/2022.
17. Prusa i3 Mk3 3D Printer, Available from: https://www.indiamart.com/proddetail/prusa-i3-mk3-3d-printer-assembled-20055373573.html, Accessed on: 04/02/2022.
18. Cau, G., Cocco, D., (2014). *Comparison of medium-size concentrating solar power plants based on parabolic trough and linear Fresnel collectors*, Energy procedia, 45, 101–110.
19. Ledo, L., Kosasih, P.B., Cooper, P., (2011). *Roof mounting site analysis for micro-wind turbines*, Renew. Energy, 36 (5), 1379–1391.
20. Abohela, I., Hamza, N., Dudek, S., (2013). *Effect of roof shape, wind direction, building height and urban configuration on the energy yield and positioning of roof mounted wind turbines*, Renew. Energy, 50, 1106–1118.
21. Balduzzi, F., Bianchini, A., Ferrari, L., (2012). *Microeolic turbines in the built environment: influence of the installation site on the potential energy yield*, Renew. Energy, 45 (1), 163–174.
22. Tabrizi, A.B., Whale, J., Lyons, T., et al., (2015). *Rooftop wind monitoring campaigns for small wind turbine applications: effect of sampling rate and averaging period*, Renew. Energy, 77, 320–330.
23. https://artillery3dexpert.fr/collections/filament-pla-premium/products/filament-pla-premium-fibre-de-carbone-1kg-1-75mm, Accessed on: 04/02/2022.
24. Huang, B., Zhao, Z., Wu, H., et al., (2018). *Near-ground impurity-free wind and wind-driven sand of photovoltaic power stations in a desert area*, J. Wind Eng. Ind. Aerod., 179, 483–502.
25. Gong, B., Wang, Z., Li, Z., et al., (2012). *Field measurements of boundary layer wind characteristics and wind loads of a parabolic trough solar collector*, Sol. Energy, 86, 1880–1898.
26. Abueiddaa, D.W., Elhebearya, M., Shianga, C.-S. (A.), Panga, S., Abu Al-Rubb, R.K., Jasiuka, I.M., (2019). *Mechanical properties of 3D printed polymeric Gyroid cellular structures: Experimental and finite element study*, Materials & Design, 165, 107597, Available from: https://www.sciencedirect.com/science/article/pii/S0264127519300176, Accessed on: 04/02/2022.
27. Kopp, G.A., Surry, D., Mans, C., (2005). *Wind effects of parapets on low buildings: Part 1. Basic aerodynamics and local loads*, J. Wind Eng. Ind. Aerod., 93, 817–843.
28. Kopp, G.A., Mans, C., Surry, D., (2005). *Wind effects of parapets on low buildings: Part 2. Structural loads*, J. Wind Eng. Ind. Aerod., 93, 843–855.
29. CR 1-1-4/2012, (2012). *Cod de proiectare. Evaluarea actiunii vantului asupra constructiilor.* Ministry of Regional Development and Tourism, Bucharest, Romania, available at: https://www.academia.edu/13392237/PROIECT_COD_DE_PROIECTARE_EVALUAREA_AC%C5%A2IUNII_V%C3%82NTULUI_ASUPRA_CONSTRUC%C5%A2IILOR.

Received: April 19, 2022 / Accepted: December 15, 2022 / Paper available online: December 20, 2022